ACS APPLIED MATERIALS & INTERFACES

Research Article

www.acsami.org

Carbon-Coated Si Nanoparticles Dispersed in Carbon Nanotube Networks As Anode Material for Lithium-Ion Batteries

Leigang Xue, Guanjie Xu, Ying Li, Shuli Li, Kun Fu, Quan Shi, and Xiangwu Zhang*

Fiber and Polymer Science Program, Department of Textile Engineering, Chemistry and Science, North Carolina State University, Raleigh, North Carolina 27695-8301, United States

ABSTRACT: Si has the highest theoretical capacity among all known anode materials, but it suffers from the dramatic volume change upon repeated lithiation and delithiation processes. To overcome the severe volume changes, Si nanoparticles were first coated with a polymer-driven carbon layer, and then dispersed in a CNT network. In this unique structure, the carbon layer can improve electric conductivity and buffer the severe volume change, whereas the tangled CNT network is expected to provide additional mechanical strength to maintain the integrity of electrodes, stabilize the electric conductive network for active Si, and eventually lead to better cycling performance. Electrochemical test result indicates the carbon-coated Si nanoparticles dispersed in CNT networks show capacity retention of 70% after 40 cycles, which is much better than the carbon-coated Si nanoparticles without CNTs.

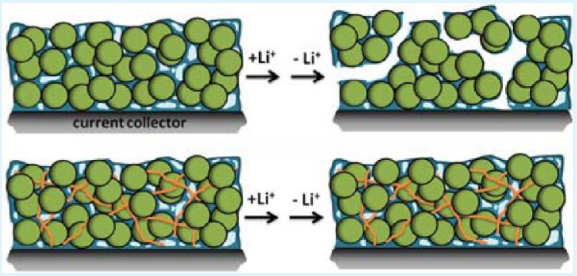

KEYWORDS: *lithium-ion battery, si-based anode, cycling stability, carbon coating, CNT networks*

1. INTRODUCTION

Si, as the second most abundant element on earth, is expected to play a significant role in the energy storage field. As a promising anode material for lithium-ion batteries (LIBs), Si provides the highest known lithium storage capacity (4200 mA h g^{-1}), which is more than 10 times greater than that of commercialized graphite (372 mA h g^{-1}).[1−3] However, the limited cycling life of Si anodes, resulting from the large volume change upon lithium insertion and extraction, greatly restricts their practical use in LIBs. Studies have shown that each silicon atom can theoretically accommodate up to 4.4 lithium atoms to form $Li_{22}Si_5$ alloy, accompanied by a volume expansion of about 400%.[4,5] Such huge volume change leads to the pulverization of electrodes, which in turn causes the breakdown of electric conductive network and insulation of active material, eventually resulting in rapid capacity fading.[6,7]

To address the large volume change, researchers have employed Si nanoparticles because they generate less stress during cycling and can better accommodate the repeated volume expansion and contraction.[8,9] For further improvement, the nanosized Si was often encapsulated in a carbon shell, which not only provides greatly improved electric conductivity, but also helps buffer the severe volume change.[10−13] However, the unstable electrode integrity due to the insufficient binder strength and significant volume change of Si is still a problem.

The failure mechanism of Si-based electrodes is illustrated in Figure 1. During the electrode fabrication process, active material such as carbon-coated Si is first made into slurry by using a polymer binder and corresponding solvent. After drying, active material particles are then connected with each other by the polymer binder to form an electrode (Figure 1a). Upon repeated volume expansion and contraction, however, the polymer binder does not have sufficient mechanical strength to maintain the integrity of the Si electrode, leading to the crack, pulverization, and breakdown of the electric conductive network of the electrode (Figure 1b). Finally, the insulation of active Si results in rapid capacity loss.

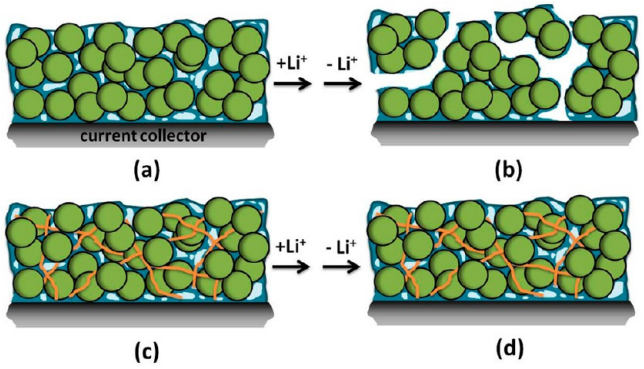

Figure 1. Schematic of a traditional Si anode composed of carbon-coated Si nanoparticles and binder (a) before and (b) after cycling, and the new Si anode composed of carbon-coated Si nanoparticles dispersed in a CNT network and binder (c) before and (d) after cycling.

In this work, carbon coating and carbon nanotube (CNT) framework were combined to improve the cycling stability of Si electrodes. As shown in Figure 1c, carbon-coated Si nanoparticles were dispersed into a network composed of carbon nanotubes

Received: July 10, 2012
Accepted: December 3, 2012
Published: December 3, 2012

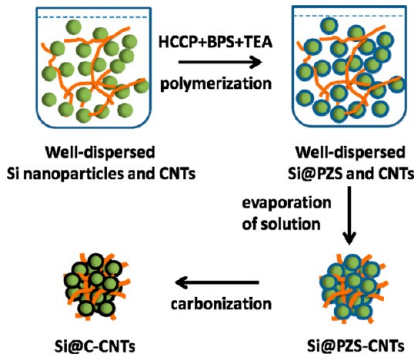

Figure 2. Schematic illustration of the preparation process of the Si@C−CNTs.

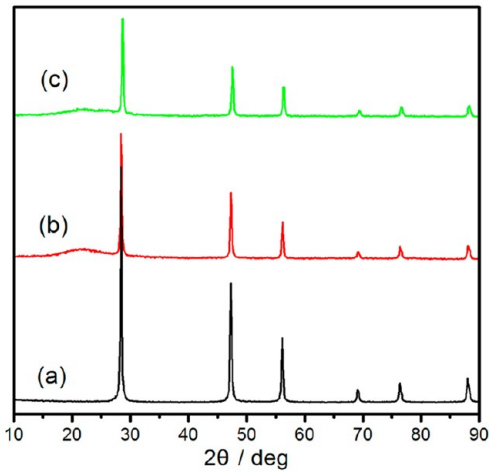

Figure 3. X-ray diffraction patterns of (a) Si nanoparticles, (b) Si@C, and (c) Si@C−CNTs.

(CNTs) and polymer binder. The CNT framework could provide additional mechanical strength to prevent the crack and pulverization of the electrode structure during repeated volume expansion and contraction, which helps maintain the integrity of the Si electrodes and the electric conductive network, and eventually leads to better cycling performance (Figure 1d). With the CNT network, the electric contact could be kept even if some cracks appear in the electrode. This paper introduces the preparation process of the carbon-coated Si nanoparticles dispersed in CNT networks (Si@C−CNTs) and investigates the electrochemical performance of the resultant electrode.

2. EXPERIMENTAL SECTION

2.1. Material Synthesis. The preparation process of Si@C−CNTs is shown in Figure 2. First, CNTs (0.025g, 6−13 nm in diameter, 2.5−20 μm in length, Aldrich), Si nanoparticles (0.10 g, 30 - 100 nm in diameter, Nanostructured and Amorphous Materials Inc.) were dispersed in a mixed solvent of tetrahydrofuran (THF) and ethanol (150 mL, 1:1 by volume). To get homogeneous distribution of CNTs, 5 drops of CNT dispersant (nanosperse AQ, NanoLab Inc.) was added in this solution. Second, hexachlorocyclotriphosphazene (HCCP, 0.10 g, Aldrich), 4,4-sulfonyldiphenol (BPS, 0.215 g, Aldrich), and triethylamine (TEA, 10 mL, Aldrich) were added to the solution and kept in the ultrasonic bath for 10 h. During this process, poly(cyclotriphosphazene-4,4′-sulfonyldiphenol) (PZS) polymer was formed on the surface of Si nanoparticles. Third, the mixture was washed with THF/ethanol solution (1:1 by volume) for 3 times, followed by solvent evaporation at 80 °C under vacuum. Finally, the resultant mixture was calcined at 900 °C in argon for 2 h and the PZS polymer was transformed to carbon layer in this carbonization process. For the purpose of comparison, carbon-coated Si nanoparticles without CNTs (Si@C) were also prepared using the same method.

2.2. Characterizations and Electrochemical Evaluation. Powder X-ray diffraction patterns were collected on a Rigaku SmartLab X-ray Diffractometer with CuKα radiation between 10 and 90° at a scan rate of 5°/min. Field-emission scanning electron microscopy (SEM, JEOL 6400) and field-emission transmission electron microscopy (TEM, Hitachi HF2000) were used to observe the morphology of the prepared samples. Elemental Analyzer (Perkin-Elmer, CHN 2400) and Energy-dispersive X-ray spectroscopy (EDX) were used to determine the composition of the as-prepared materials.

Electrochemical performance evaluations were performed using lithium-ion half cells. The Si@C and Si@C−CNTs working electrodes were prepared by mixing 80% active material and 20% polyamideimide (PAI) binder dissolved in N-methylpyrrolidinone (NMP). No additional conductive carbon additives were used. For comparison, Si working electrodes were prepared by mixing 80% Si nanoparticles, 10% BTY-175 conductive carbon (Blue nano Inc.) and 10% PAI dissolved in NMP. The slurries were coated onto Cu foil. After coating, the electrodes were dried at 80 °C for 12 h, and weighed before assembly. The typical mass load of the active material was about 2 mg cm^{-2}. Using the above

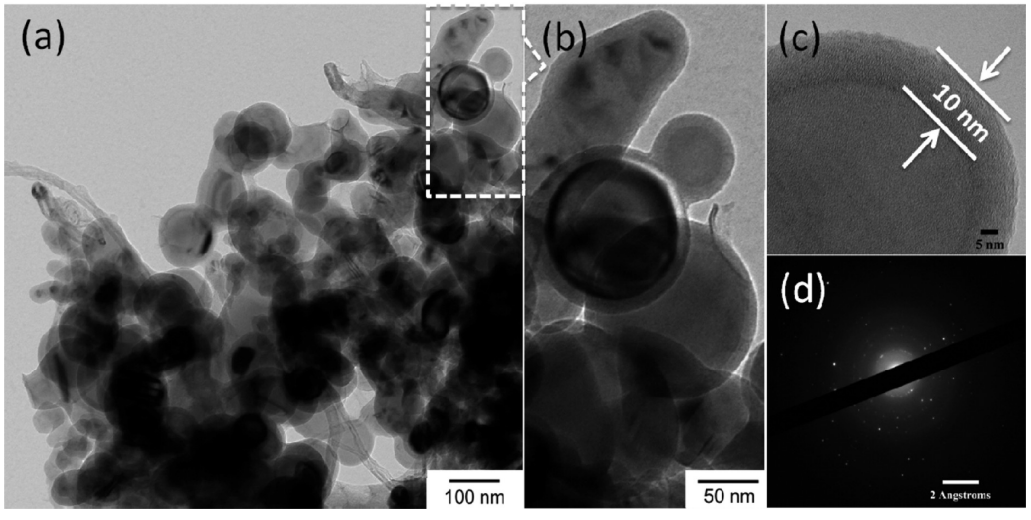

Figure 4. (a−c) TEM images of Si@C−CNTs with different magnifications, and (d) selected area electron diffraction (SAED) pattern.

dx.doi.org/10.1021/am3027597 | ACS Appl. Mater. Interfaces 2013, 5, 21−25

electrodes, 2032 type coin cells (20 mm diameter, 3.2 mm thickness) were assembled in an argon glovebox with lithium as the counter electrode, Celgard 2400 membrane as the separator, and 1 M $LiPF_6$/EC+DMC+DEC (1:1:1 by volume, MTI Corporation) as the electrolyte. Cyclic voltammetry (CV) measurements were conducted with a Gamry Reference 600 between 2 V and 0.02 V with a scan rate of 0.05 mV/s. Charge/discharge experiments were performed using a LAND CT2001A Battery Testing System.

3. RESULTS AND DISCUSSION

Figure 3 shows the XRD patterns of the Si nanoparticles, Si@C, and Si@C−CNTs. From Figure 3a, it is seen that Si nanoparticles present well-defined peaks at 2θ of 28.4, 47.4, 56.2, 69.2, 76.5, and 88.1°, which are assigned to the (111), (220), (311), (400), (331), and (422) planes of crystallized Si, respectively (JCPDS No. 27−1402). After heat treatment at 900 °C in argon, the Si nanoparticles coated by carbon are still crystalline since no apparent changes can be observed for Si peaks. One broad peak appears at around 24° (Figure 3b, c), indicating that the carbon coating is amorphous, as suggested by previous reports.[14,15] In addition, there is no apparent difference between XRD patterns of Si@C and Si@C−CNTs.

The TEM image (Figure 4a) of Si@C−CNTs clearly demonstrates the coexistence of three phases, i.e., the crystalline Si phase, the amorphous carbon coating, and CNTs. The Si nanoparticles are mixed with CNTs, and almost each individual Si nanoparticle has been coated homogeneously with carbon layer. From higher magnification (Figure 4b, c), it can be confirmed that the diameter of Si nanoparticles is 30−100 nm and the thickness of the amorphous carbon coating layer is about 10 nm. The carbon layer closely sticks to the particle surface and there is no vacant space between the carbon "shell" and silicon "core", but it is still expected to provide good electric conductivity and help buffer the volume change of Si.[12,16,17] The carbon layer does not present any ordered structure, which is in agreement with the amorphous carbon structure revealed by the XRD analysis (Figure 4c) The crystalline structure of Si is also confirmed by the spot pattern in selected area electron diffraction (SAED), as shown in Figure 4d.

Figure 5a shows an overall view of the carbon-coated Si nanoparticles dispersed in a CNT network. It is seen that some

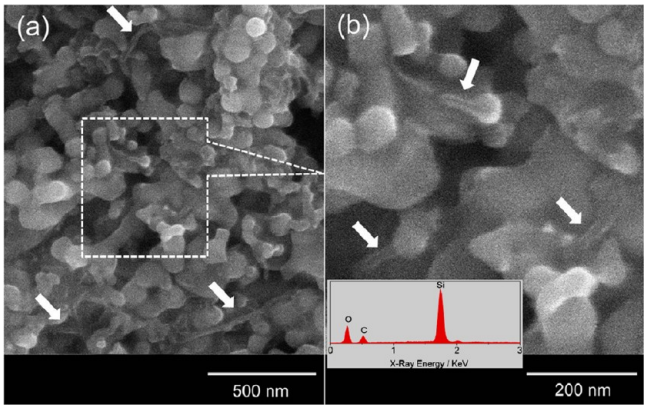

Figure 5. SEM images of Si@C−CNTs with different magnifications, and corresponding energy-dispersive X-ray spectroscopy (EDX, inset in b).

sections of the long CNTs (2.5−20 μm in length) are exposed (marked with white arrows), and the remaining tubes are blocked by Si nanoparticles. At higher magnification (Figure 5b), shorter sections of CNTs can be seen. Energy-dispersive X-ray

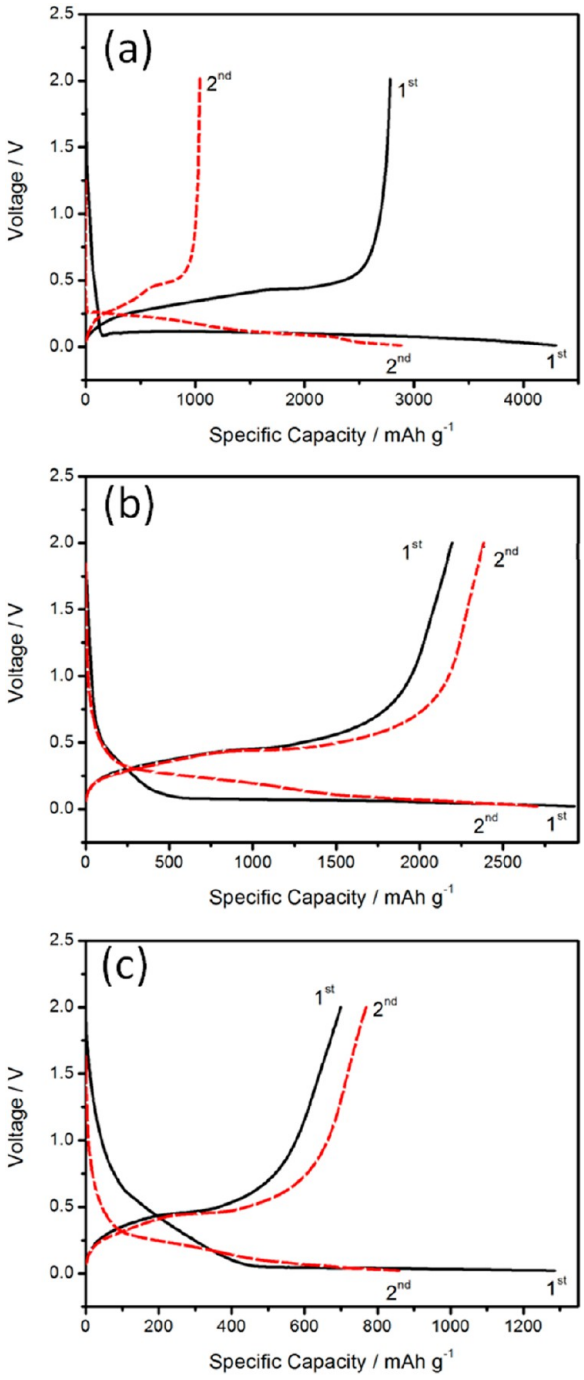

Figure 6. Charge/discharge curves of (a) Si, (b) Si@C, and (c) Si@C−CNTs at 100 mA g^{-1} and within a voltage window of 0.02−2.0 V.

spectroscopy (inset in Figure 5b) was also obtained to provide the composition information of this material, and it is found that the peaks of Si and C can be clearly seen and the carbon content (including carbon coating and CNTs) is 52.3%. From the SEM and TEM characterizations, it can be concluded that the Si nanoparticles are uniformly coated with carbon and they are well dispersed in the CNT network, just as described in the schematic illustration (Figure 1c). In this work, the CNTs dispersed in carbon-coated Si nanoparticles are expected to provide additional mechanical strength to help maintain the electrode integrity and provide stable electric conductive network. In many recent reports, Si/C composite nanofibers were

dx.doi.org/10.1021/am3027597 | ACS Appl. Mater. Interfaces 2013, 5, 21−25

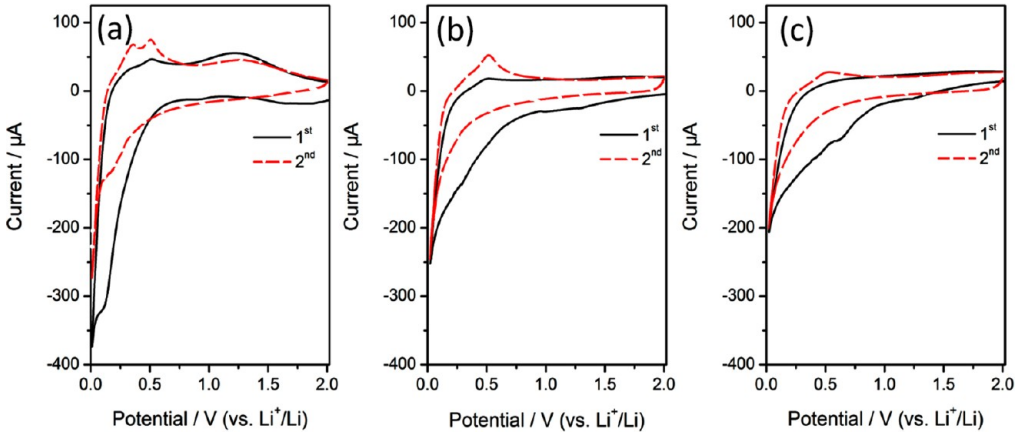

Figure 7. Cyclic voltammetry curves of (a) Si, (b) Si@C, and (c) Si@C−CNTs between 2 and 0.02 V with a scan rate of 0.05 mV/s.

prepared by electrospinning to strengthen the electrode integrity and improve the cycling performance.[18−23] From SEM and TEM characterizations shown in these reports,[18−21] however, a significant amount of Si nanoparticles were found on the fiber surface and they have the tendency to loss contact with carbon nanofibers during cycling. In this work, the carbon coating and CNTs work together to achieve high electrode integrity and provide good electric conductive network for Si.

Galvanostatic charge−discharge test was carried out at a current density of 100 mA g^{-1} within a voltage window of 0.02−2.0 V. Charge/discharge curves of pristine Si nanoparticles are shown in Figure 6a. A distinct plateau at about 100 mV can be observed and this can be attributed to the lithium alloying with crystalline Si nanoparticles.[24,25] It was reported that the alloying process in Si anodes results in the successive formation of $Li_{12}Si_7$, $Li_{14}Si_6$, $Li_{13}Si_4$, and eventually $Li_{22}Si_5$ alloy.[5] Upon the following delithiation process of Si, two plateaus at around 250 and 450 mV can be observed. The initial discharge and charge capacities of Si are 4299 and 2780 mA h g^{-1}, respectively, corresponding to a Coulombic efficiency of 65%. The relatively low initial Coulombic efficiency of pristine Si can be attributed to the drastic volume changes and the loss of electric contact between Si nanoparticles, which in turn leads to large irreversible capacity. After the first cycle, the discharge potential plateau shifts to about 0.2 V because the crystalline Si phase turns into an amorphous phase.[26−28]

The charge/discharge curves of Si@C are shown in Figure 6b. In addition to the potential plateau at 100 mV, an obvious step can also be observed between 0.60 and 0.10 V, in which the passivation film, also known as the solid/electrolyte interphase (SEI), is formed by the irreversible reduction of electrolyte on the surface of the carbon layer. The initial discharge and charge capacities of Si@C are 2928 and 2195 mAh g^{-1}, respectively, corresponding to a Coulombic efficiency of 75%. It should be noted that the Coulombic efficiency is improved after carbon coating even if an obvious irreversible SEI formation process is observed between 0.60 and 0.10 V. Generally, the introduction of amorphous carbon gives rise to larger irreversible capacity because of the severe SEI formation on the surface of amorphous carbon.[15] In this material, however, the initial Coulombic efficiency was improved, which should be attributed to the volume buffer effect of carbon layer and the better electric conductive network.

The Si@C−CNTs (Figure 6c) shows a similar charge/discharge characteristic to that of Si@C. The initial discharge and charge capacities of Si@C−CNTs are 1286 and 699 mAh g^{-1}, respectively. The introduction of CNTs leads to lower capacity because of the lower capacity of CNTs than Si. The contribution of the first potential plateau (0.60−0.10 V, SEI formation) in the first lithiation process becomes larger, resulting in a lower initial Coulombic efficiency of 54%. The relatively low initial Coulombic efficiency of Si@C−CNTs can be attributed to the low Coulombic efficiency of CNTs.[29−31]

Cyclic voltammetry (CV) measurements were carried out on Si nanoparticles, Si@C, and Si@C−CNTs, respectively (Figure 7). Figure 7a shows the first two cycles of Si nanoparticles between 0.02 and 2.0 V with a scan rate of 0.05 mV/s. As the potential scans cathodically from 2.0 to 0.02 V at the first cycle, a reduction peak of crystalline Si can be found at around 100 mV. In the following anodic scan, two oxidation peaks appear at 250 and 450 mV, respectively, which reflect the delithiation process of Si. For Si@C, a peak at 0.32 V in cathodic scan can be clearly seen because of the SEI formation on the carbon surface. For the Si@C−CNTs material, the SEI formation shifts to 0.6 V due to the introduction of CNTs. The CV results are in agreement with the charge/discharge curves.

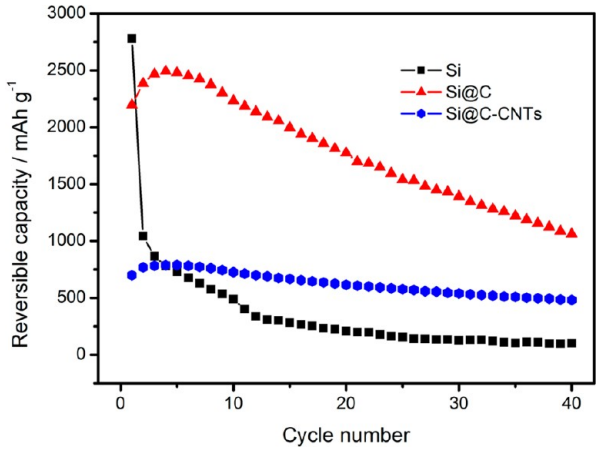

Figure 8. Cycling performance of Si, Si@C, and Si@C−CNTs at 100 mA g^{-1} and within a voltage window of 0.02−2.0 V.

The cycling performance of Si, Si@C and Si@C−CNTs are shown in Figure 8. Here, all capacities were calculated on the basis of the total weight of composite material including carbon

dx.doi.org/10.1021/am3027597 | ACS Appl. Mater. Interfaces 2013, 5, 21−25

coating, CNTs, and Si. The percent ratio of Si and carbon in Si@C material is 61.0:29.6, and the percent ratio of Si, CNT, and carbon in Si@C−CNTs material is 33.2:8.3:46.0. The Si electrode exhibits a poor cycling performance. Although it shows a very high reversible capacity of 2780 mA h g^{-1} in the first cycle, the Si electrode delivers only 100 m Ah g^{-1} capacity after 40 cycles. After carbon coating, the resultant Si@C shows much better cycling stability because there is a homogeneous carbon layer on the surface of the Si nanoparticles to buffer the volume change and provide good electric conductivity. As a result, the Si@C anode shows capacity retention of 48% after 40 cycles. For Si@C−CNTs, a small increase of reversible capacity is observed during the first 5 cycles. After 5 cycles, the capacity starts to fade slowly. Although it shows much lower capacity (699 mA h g^{-1}) than the other two electrodes due to the introduction of carbon layer and CNTs, the Si@C−CNTs material exhibits the best cycling stability among all three anodes and the capacity retention after 40 cycles is 70%. According to the previous report,[32] any anode capacity greater than 1000 mA h g^{-1} will not lead to improvement in the battery performance due to the limitation in the cathode capacity (<250 mA h g^{-1}), which is significantly lower than the anode capacities. Therefore, the capacity (699 mA h g^{-1}) achieved by Si@C−CNTs is compatible with the current cathode materials.

4. CONCLUSIONS

Si nanoparticles were uniformly coated with amorphous carbon and well-dispersed in CNT networks. The unique structure was designed in order to buffer the severe volume change and maintain a stable electric conductive network for active Si. Three kinds of Si-based anode materials: Si, Si@C and Si@C−CNTs, have been investigated. Galvanostatic charge−discharge tests show that the cycling stability can be improved by coating the Si nanoparticles with a carbon layer, and it can be further improved by dispersing the carbon-coated Si nanoparticles into a CNT network. The tangled CNT network in the electrode can help prevent crack and pulverization, maintain the integrity of electrodes, and stabilize the electronic conductive network, eventually leading to better cycling performance.

AUTHOR INFORMATION

Corresponding Author

*E-mail: xiangwu_zhang@ncsu.edu.

Notes

The authors declare no competing financial interest.

ACKNOWLEDGMENTS

This research was supported by the U.S. Department of Energy under Grant DE-EE0001177, Advanced Transportation Energy Center, and ERC Program of the National Science Foundation under Award EEC-08212121.

REFERENCES

(1) Magasinki, A.; Dixon, P.; Hertzberg, B.; Kvit, A.; Ayala, J.; Yushin, G. *Nat. Mater.* **2010**, *9*, 353.
(2) Cahen, S.; Janot, R.; Laffont-Dantras, L.; Tarascon, J. M. *J. Electrochem. Soc.* **2008**, *155*, A512.
(3) Li, H.; Huang, X. J.; Chen, L. Q.; Wu, Z. G.; Liang, Y. *Electrochem. Solid-State Lett.* **1999**, *2*, 547.
(4) Sharma, R. A.; Seefurth, R. N. *J. Electrochem. Soc.* **1976**, *123*, 1763.
(5) Boukamp, A.; Lesh, G. C.; Huggins, R. A. *J. Electrochem. Soc.* **1981**, *128*, 725.
(6) Poizot, P.; Laruelle, S.; Grugeon, S.; Dupont, L.; Tarascon, J. M. *J. Power Sources* **2001**, *97*, 235.
(7) Huggins, R. A. *J. Power Sources* **1999**, *81*, 1319.
(8) Dimitrijevic, B. J.; Aifantis, K. E.; Hackl, K. *J. Power Sources* **2012**, *206*, 343.
(9) Guo, Z. P.; Wang, J. Z.; Liu, H. K.; Dou, S. X. *J. Power Sources* **2005**, *146*, 448.
(10) Gao, P. F.; Fu, J. W.; Yang, J.; Lv, R. G.; Wang, J. L.; Nuli, Y. N.; Tang, X. Z. *Phys. Chem. Chem. Phys.* **2009**, *11*, 11101.
(11) Ng, S. H.; Wang, J. Z.; Wexler, D.; Chew, S. Y.; Liu, H. K. *J. Phys. Chem. C* **2007**, *111*, 11131.
(12) Ng, S. H.; Wang, J.; Wexler, D.; Konstantinov, K.; Guo, Z. P.; Liu, H. *Angew. Chem., Int. Ed.* **2006**, *45*, 6896.
(13) Si, Q.; Hanai, K.; Imanishi, N.; Kubo, M.; Hirano, A.; Takeda, Y.; Yamamoto., O. *J. Power Sources* **2009**, *189*, 761.
(14) Noh, M.; Kwon, Y.; Lee, H.; Cho, J.; Kim, Y.; Kim, M. G. *Chem. Mater.* **2005**, *17*, 1926−1929.
(15) Kim, C.; Yang, K. S.; Kojima, M.; Yoshida, K.; Kim, Y. J.; Kim, Y. A.; Endo, M. *Adv. Funct. Mater.* **2006**, *16*, 2393.
(16) Kwon, Y.; Cho, J. *Chem. Commun.* **2008**, 1109.
(17) Hu, Y. S.; Demir-Cakan, R.; Titirici, M. M.; Müller, J. O.; Schlögl, R.; Antonietti, M.; Maier, J. *Angew. Chem., Int. Ed.* **2008**, *47*, 1645.
(18) Ji, L. W.; Zhang, X. W. *Energy Environ. Sci.* **2010**, *3*, 124.
(19) Ji, L. W.; Zhang, X. W. *Carbon* **2009**, *47*, 3219.
(20) Ji, L. W.; Jung, K. H.; Medford, A. J.; Zhang, X. W. *J. Mater. Chem.* **2009**, *19*, 4992.
(21) Ji, L. W.; Zhang, X. W. *Electrochem. Commun.* **2009**, *11*, 1146.
(22) Lee, B. S.; Son, S. B.; Park, K. M.; Seo, J. H.; Lee, S. H.; Choi, I. S.; Oh, K. H.; Yu, W. R. *J.Power Sources* **2012**, *206*, 267.
(23) Hwang, T. H.; Lee, Y. M.; Kong, B. S.; Seo, J. S.; Choi, J. W. *Nano Lett.* **2012**, *12*, 802.
(24) Chan, C. K.; Peng, H. L.; Liu, G.; Mcilwrath, K.; Zhang, X. F.; Huggins, R. A.; Cui, Y. *Nature Nanotechnol.* **2008**, *3*, 31.
(25) Limthongkul, P.; Jang, Y. I.; Dudney, N. J.; Chiang, Y. M. *Acta Mater.* **2003**, *51*, 1103.
(26) Netz, A.; Huggins, R. A.; Weppner, W. *J. Power Sources* **2003**, *119−121*, 95.
(27) Li, J.; Dahn, J. R. *J. Electrochem. Soc.* **2007**, *154*, A156.
(28) Obrovac, M. N.; Krause, L. J. *J. Electrochem. Soc.* **2007**, *154*, A103.
(29) Guo, Z. P.; Zhao, Z. W.; Liu, H. K.; Dou, S. X. *Carbon* **2005**, *43*, 1392.
(30) Park, M. S.; Needham, S. A.; Wang, G. X.; Kang, Y. M.; Park, J. S.; Dou, S. X.; Liu, H. K. *Chem. Mater.* **2007**, *19*, 2406.
(31) Chen, W. X.; Lee, J. Y.; Liu, Z. L. *Carbon* **2003**, *41*, 959.
(32) Kasavajjula, U.; Wang, C.; Appleby, A. J. *J. Power Sources* **2007**, *163*, 1003.